

The coherence of quantum dot confined electron- and hole-spin in low external magnetic field

Dan Cogan,¹ Zu-En Su,¹ Oded Kenneth,¹ and David Gershoni^{1, *}

¹*The Physics Department and the Solid State Institute,
Technion–Israel Institute of Technology, 3200003 Haifa, Israel*

We investigate experimentally and theoretically the temporal evolution of the spin of the conduction band electron and that of the valence band heavy hole, both confined in the same semiconductor quantum dot. In particular, the coherence of the spin purity in the limit of a weak externally applied magnetic field, comparable in strength to the Overhauser field due to fluctuations in the surrounding nuclei spins. We use an all-optical pulse technique to measure the spin evolution as a function of time after its initialization. We show for the first time that the spin purity performs complex temporal oscillations which we quantitatively simulate using a central spin model. Our model encompasses the Zeeman and the hyperfine interactions between the spin and the external and Overhauser fields, respectively. Our novel studies are essential for the design and optimization of quantum-dot-based entangled multi-photon sources. Specifically, cluster and graph states, which set stringent limitations on the magnitude of the externally applied field.

Semiconductor quantum-dot-based devices are currently the most viable technology for generating quantum light for future quantum information and network applications. They are easily incorporated into electro-optical classical components [1–5] while demonstrating unparalleled efficiency, photon extraction rates [4–6], and high quality, nearly transform-limited photon indistinguishability [5–8]. Furthermore, a quantum dot (QD) acts like a single atom emitter and thus can be a source of entangled photons via its spontaneous emission [9–11].

One particularly important resource for quantum communication is a multi-photonic entangled state - a cluster or a graph state [12–15]. Schemes that rely on entangling the spin degree of freedom of QD confined charge carriers with the polarization degree of freedom of the photons that QD emit have been proposed [16, 17] and experimentally demonstrated [18]. These schemes use a single spin precessing in an externally applied magnetic field while being driven by a sequence of precisely timed short laser pulses. Upon each excitation of the QD spin, a single photon is spontaneously emitted, and the photon's polarization is entangled with the state of the de-excited spin. This process can be performed many times to generate a large cluster of entangled photons.

Schwartz and coworkers[18] used the QD-confined dark-exciton (DE) as entangler. The DE has an integer total spin (2) and the short-range exchange interaction between its electron and hole removes its spin degeneracy [19]. As a result, no external field is required for the DE to precess and be used as an entangler[18].

There are, however, advantages for using the electron or even better, the heavy hole, which has comparable spin coherence time to that of the DE [20], as an entangler. Single carriers as opposed to the DE, have half integer total spin (1/2 and 3/2, respectively) and therefore in the absence of external field are Kramers' degenerate. Therefore, an external field is required for them to precess, and its magnitude can be utilized to accurately tune the pre-

cession period. This allows optimization of the entanglement robustness and the generation rate of the entangled multiphotons [18]. Moreover, in the single carrier case the emitted photons are indistinguishable [21, 22]. This is true as long as the the external field-induced Zeeman-splitting of the spin states are smaller than the spectral width of the emitted photons. In this particular regime, the Zeeman interaction is comparable in magnitude to the hyperfine interaction induced by the surrounding nuclei spins. Thereby, one must consider both interactions in designing QD based devices as entangled light sources.

Studies of the central-spin evolution under the influence of the hyperfine and quadrupole interactions with the nuclei were recently published [20, 23]. Few distinct temporal domains in the central spin evolution were observed. During the first temporal domain, which is relevant to this work, the Overhauser field, due to frozen fluctuations in the nuclei spins, can be considered static and the central spin precesses about this field direction.

In this work, we study experimentally and theoretically the central-spin evolution and decoherence mechanism of both the QD confined electron [24, 25] and heavy-hole (HH) [26–32] spins. We vary the ratio between the magnetically induced Zeeman interaction and the hyperfine interaction with the central spin and measure the temporal evolution of the spin purity.

In addition to its scientific importance, this work provides tools for state tomography, engineering and optimizing QDs based devices for generating photonic cluster and graph states. These multiphoton entangled states are important resources for quantum repeaters and entanglement distribution [12–15], enabling implementations of quantum information communication protocols.

The primary decoherence mechanism of electronic spin qubits in QDs is the hyperfine-interaction with the $\sim 10^5$ nuclei spins in the QD [33–36]. The Zeeman interaction with the external field does not cause decoherence but induces coherent precession around the field direction.

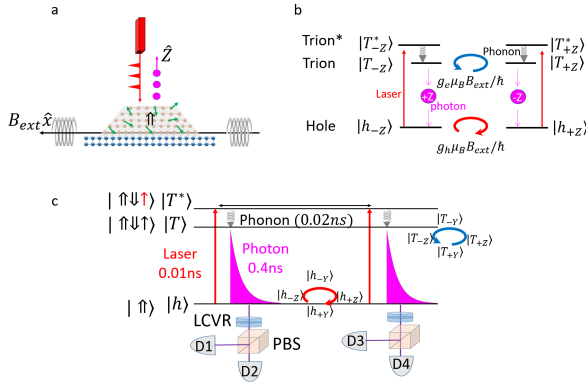


Figure 1. a) The QD sample. 12 ps laser π -pulses (marked in red) resonantly excite the central spin. The excited spin then returns to its ground state by emitting single photons (pink circles). The spin evolves under the joint influence of the external and nuclear magnetic fields. Green arrows represent the randomly distributed nuclear spins. b) The polarization selection rules for the hole-Trion optical transition. $\pm Z$ is the polarization of the exciting laser and the emitted photons. c) The experimental setup for initializing and probing the central spin evolution. Liquid-crystal-variable-retarders (LCVR's) and polarizing beam-splitters (PBSs) are used to project the photons polarization. By selecting the polarization of the exciting pulses and that of the projected photons, while setting the time difference between the pulses, one can fully investigate the electron and hole spins evolution.

The two interactions can be described by a Hamiltonian

$$H = \frac{1}{2} \vec{C} \cdot \hat{\sigma} \quad (1)$$

acting on the electronic spin, with $\hat{\sigma}$ being the Pauli matrices describing the spin. $\vec{C} = \bar{g}\mu_B\vec{B}_{ext} + \bar{\gamma}\vec{B}_N$ is the joint Zeeman and hyperfine interactions, where \bar{g} and $\bar{\gamma}$ are the Lande-factor and hyperfine interaction tensors, \vec{B}_{ext} and \vec{B}_N are the external and Overhauser field. The Overhauser field is treated as random, having Gaussian distribution with zero mean and a variance σ (not to be confused with the Pauli matrices). Defining a modified unitless magnetic field $\vec{B} = \vec{B}_N/\sigma$ with root mean square of one and redefining the tensor $\bar{\gamma}$ having energy units, the corresponding probability distribution then takes the standard form $dP(B) = \frac{1}{(2\pi)^{3/2}} \exp(-\frac{1}{2}B^2) d^3B$.

While the conduction-electron interaction with the nuclei, which we denote by γ_e , is mostly isotropic [34], the interaction of the valence heavy-hole for which the orbital momentum and the spin are aligned with the growth direction is anisotropic [36]. We denote by γ_{h_z} (γ_{h_p}) the interaction of the valence heavy-hole spin with the Overhauser field component along (perpendicular to) the growth axis \hat{z} [20]. Defining the externally applied magnetic field B_{ext} as the x-direction, and assuming that the tensors g and γ are diagonal (see SM) the vector C is

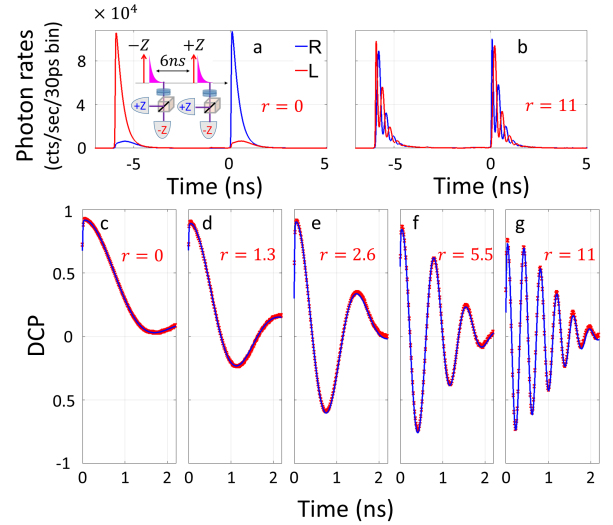


Figure 2. Measurements of the Trion spin-evolution. Polarization sensitive time-resolved PL emission from the positive trion transition for a Zeeman-Hyperfine ratio (Eq. 2) of a) $r = 0$, and b) $r = 11$. The inset in a) describes the pulse (red arrows) and detection (magenta markings) sequence used for these measurements. The trion spin is alternately initialized to spin down and up to prevent buildup of Overhauser-field in the sample. c) - g) Time resolved degree of circular polarization (D_{cp} , Eq. 4) of the PL emission for various r parameters. Red marks represent the measured data and the overlaid blue lines represent our central-spin model best fits (see SM). From these multiple fits, we deduce the electron's g-factor g_e , the interaction radiative energy with the nuclear environment γ_e , and the Trion's radiative time τ_{photon} , as summarized in Table. 1.

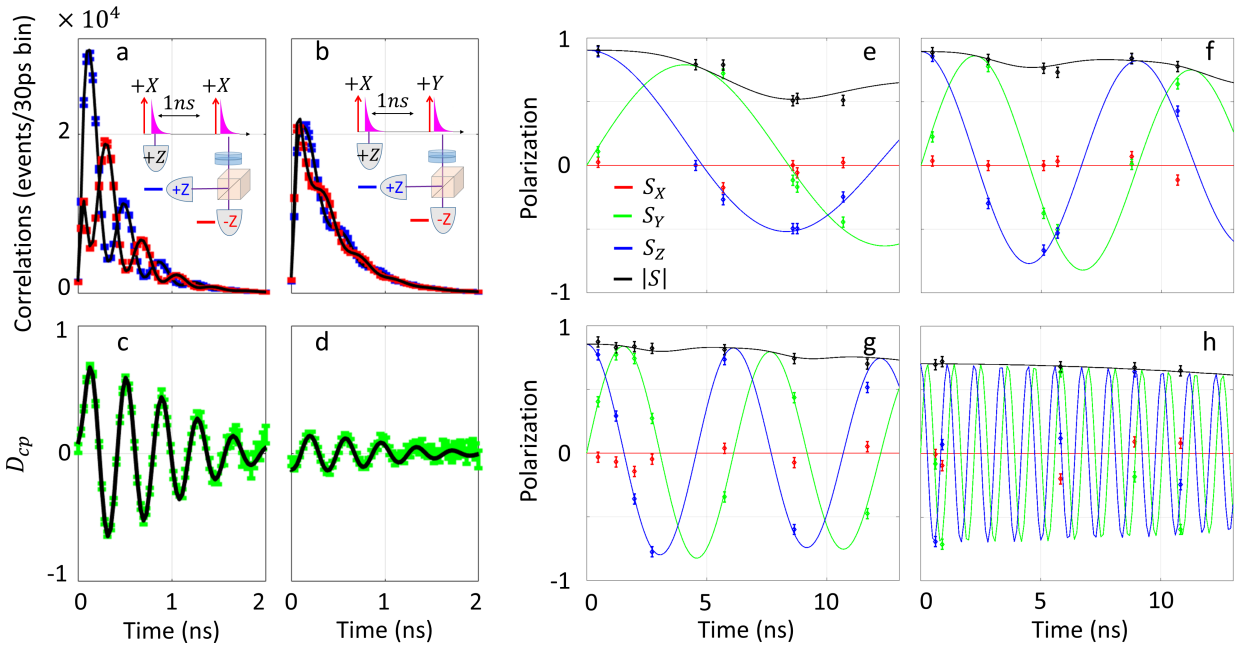
given by:

$$\vec{C} = [g_x\mu_B B_{ext} + \gamma_x B_x, \gamma_y B_y, \gamma_z B_z].$$

and we use it to derive expressions for the temporal evolution of both the heavy-hole and electron spins (see SM). We then investigate the spin evolution of both carriers for various external field strengths, affecting the Zeeman to Hyperfine interaction ratio:

$$r = C_{zeeman}/C_{hf}^{\perp} = \frac{g_x\mu_B B_{ext}}{\sqrt{\gamma_y^2 + \gamma_z^2}}. \quad (2)$$

We mark the HH spin along the shortest axis of the QD's 3-D potential trap (marked +Z in Fig. 1a) by $|\uparrow\rangle$ ($|\downarrow\rangle$) for spin up (down) state. Resonantly tuned laser pulse photogenerates an extra electron-hole pair in the QD, converting the HH to a positive Trion ($|\uparrow\downarrow\rangle$). The ground level of the positive trion is composed of two paired HHs with opposite spins and a single conduction band electron. The selection rules for optical transitions between the HH states and that of the trion form a



π -system [20] with the following optical transitions:

$$\begin{aligned} |\uparrow\rangle &\xleftrightarrow{|-Z\rangle} |\uparrow\downarrow\uparrow\rangle, \\ |\downarrow\rangle &\xleftrightarrow{|+Z\rangle} |\downarrow\uparrow\downarrow\rangle. \end{aligned} \quad (3)$$

where $|+Z\rangle$ and $| -Z\rangle$ denote the right- and left-hand circular polarization states of the photon inducing the optical transition between the ground level qubit (HH) and the excited qubit (Trion), as described in Fig. 1b.

We note that this system allows us to investigate both the valence band HH and the conduction band electron as central spins. The HH is investigated through the ground level qubit while the electron through the excited level trion. The magnetic interaction (Eq. 1) for the paired HH spins vanishes, leaving only the electron to consider [20].

Fig. 1a and 1b show a schematic description of the InAs in GaAs self-assembled QD sample and the polarization selection rules for the hole-Trion optical transition, respectively. The externally applied in-plane magnetic field

induces coherent evolution of the central spins, which precess between their spin-up and spin-down states. The interaction of the electronic spin with the nuclear spin environment inflicts decoherence on the evolving central spins.

We use two-laser-pulses to initialize and to probe the HH and the trion qubits as described in Fig. 1c. Each laser pulse excites the HH to an excited-positive-trion level, where the unpaired electron is in its respective second energy level. The excited electron decays to its ground level forming a ground level trion by emitting an optical phonon within about $\sim 20ps$. The trion then decays radiatively by emitting a photon within about $400ps$. We project the photon's polarization using pairs of liquid-crystal-variable-retarders (LCVRs) followed by polarizing beam-splitters (PBS), transmission gratings for spectral filtering and superconducting single-photon counters for detection. The overall system efficiency is about 1% and its temporal resolution is about $30ps$. We initialize the HH and trion spin qubits by controlling

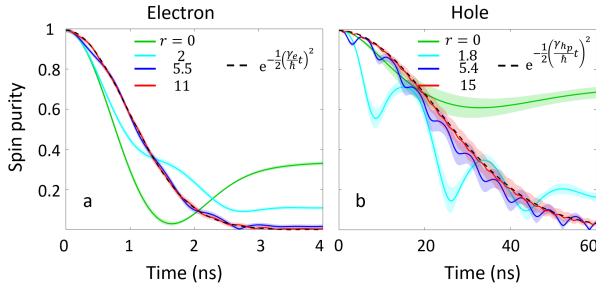


Figure 4. Model calculated central spin purity $|S(t)| = \sqrt{S_x^2(t) + S_y^2(t) + S_z^2(t)}$ vs. time for a) the electron, and b) the heavy-hole. The spin purity is calculated using the central spin model (see SM and Table. I). The spin is initialized in the z-direction ($S_z(0) = 1$) and the external field is applied in the x-direction. The colored lines represent the purity vs. time from initialization for various Zeeman-Hyperfine ratios r (Eq. 2). The shaded areas represent the uncertainties in the measured values of Table. I. The calculations result from Fig. 2 for the electron and Fig. 3 for the hole. The dash black line represents the analytic solution $|S(t)| = e^{-\frac{1}{2}(\frac{\gamma_e}{\hbar}t)^2}$ describing the purity in the limit $r \gg 1$.

Table I. The QD g-tensor and hyperfine-tensor components. Here γ_{h_p} , γ_{h_z} , and γ_e are the interaction energies of the hole and electron spins with the nuclear spin environment and g_h^x and g_e^x are the relevant HH and electron g-tensor components. The positive Trion radiative time is τ_{photon} .

	This work	Literature
γ_{h_p}	$0.029 \pm 0.005 \mu eV$	0.031[20], 0.047[28]
γ_{h_z}	$0.12 \pm 0.02 \mu eV$	0.11[20], 0.081[28]
γ_e	$0.693 \pm 0.006 \mu eV$	0.34[20], 0.33[23]
g_h	-0.128 ± 0.002	
g_e	0.367 ± 0.004	
τ_{photon}	$0.398 \pm 0.004 ns$	

the polarization of the resonant laser pulses. At the same time we also probe the state of these qubits by measuring the polarization of the emitted photons.

Fig. 2 describes how we measure the spin evolution of the positive trion. We initialize the trion qubit to spin-up and spin-down states alternately using -Z and +Z polarized 12 ps long laser π -pulses. This is done in order to avoid the accumulation of unwanted Overhauser-field [20, 38–41]. We then monitor the spin evolution during the optical recombination by projecting the emitted photon on -Z and +Z polarization basis. Fig. 2a - 2b show the time-resolved PL emission of the emitted photons for $r = 0$ and $r = 11$, respectively. Since the trion in the $|T_{+Z}\rangle$ state emits -Z photon while $|T_{-Z}\rangle$ state emits +Z photon, the spin evolution of the trion can be deduced from the polarization sensitive time resolved PL. For the Zeeman-Hyperfine ratio $r = 11$ case (Eq. 2), the

trion's spin-precession around the external magnetic field is clearly visible, while for the $r = 0$ case, one can only observe the exponential radiative decay. To increase this measurement's sensitivity, we look at the degree of circular polarization (D_{cp}) of the emission defined by

$$D_{cp}(t) = \frac{I_{+Z}(t) - I_{-Z}(t)}{I_{+Z}(t) + I_{-Z}(t)}, \quad (4)$$

where $I_{+Z}(t)$ ($I_{-Z}(t)$) denotes the measured polarized PL intensity. The $D_{cp}(t)$ distills the information on the spin evolution from the characteristic exponential radiative decay [20, 37]. Using Eq. 3, it is straightforward to show that the $D_{cp}(t)$ measures the trion's spin projection on Z-axis - $S_z(t)$.

Fig. 2c-g shows the measured $D_{cp}(t)$ for five different r cases. For $r = 0$, the spin polarization evolves only due to the Hyperfine interaction. It first decays within $\sim 1.65 ns$ and then revives back to $1/3$ of its initial value [20, 23, 34]. For $r > 0$, the spin evolves around the vector sum of \vec{B}_{ext} and \vec{B}_N . One notes that stronger external fields (higher r) result in a decrease of the initial spin polarization ($S_z(0) = 0.92$ for $r=0$, $S_z(0) = 0.71$ for $r=11$). This decrease is due to the detectors' finite temporal resolution ($\sim 30 ps$).

In Fig. 3e-h we similarly present the measured HH-spin temporal evolution for four different r ratios. The hole state is initialized to -Z state by projecting the first photon on +Z polarization. For measuring the HH spin state as a function of time after this initialization we utilize a measurement technique which provides a full tomography of the HH spin [37]. Fig. 3a-d demonstrates the application of this technique 1ns after initialization. The evolving hole state is promoted to the trion state by a second 1ns-delayed π -pulse, linearly polarized +X (Horizontal), and +Y (Diagonal). +X polarized pulse promotes an arbitrary hole spin state $\alpha |h_{+Z}\rangle + \beta |h_{-Z}\rangle$ to the trion state: $\alpha |T_{+Z}\rangle + \beta |T_{-Z}\rangle$, while +Y polarized pulse results in a $\alpha |T_{+Z}\rangle + i\beta |T_{-Z}\rangle$ trion. The D_{cp} of the emission as a function of time for both cases provide the means for a full tomography of the HH spin state at the second excitation pulse [37]. The tomography or the HH spin projections $S_x(t)$, $S_y(t)$, and $S_z(t)$, for $t=1ns$, can be quite faithfully extracted from the best fitted model calculations to the measured points in Figs. 3a-d. These fits are presented by the solid black lines overlaid on the experimental measurements.

In Fig. 3e-h, we present by red, green, and blue, the measured $S_x(t)$, $S_y(t)$, and $S_z(t)$, respectively, for various r ratios. The black points represent the spin purity which we define as $|S| = \sqrt{S_x^2 + S_y^2 + S_z^2}$. The color matched solid lines represent the calculated values (see SM) using the parameters in Table. I

In Fig. 4 we present the model-calculated time-resolved purity of the electron (in a) and HH (in b) spins, for various Zeeman-Hyperfine ratios r (see Eq. 2). The shaded

areas represent one standard deviation of the model's uncertainties in the measured Table. I values. For $r = 0$, the spin depolarizes, reaches minimum and then partially revives. Spin precession around the frozen fluctuation of the nuclear field adequately describes this observation [20, 23, 34]. Since we initialize the spin in the z -direction, γ_x and γ_y are the only relevant hyperfine tensor components contributing to the central spin depolarization. γ_z , in contrast, pins the spin to its initial direction. Consequently, the spin reaches minimum within $t_{min} = \hbar / (2(\gamma_x + \gamma_y))$, with \hbar being the plank constant. This time is given by the hyperfine-induced spin precession perpendicular to the initialization direction. In addition, the value that the purity reaches after the revival depends on the ratio between γ_z and $\gamma_x + \gamma_y + \gamma_z$. Since the hyperfine tensor is isotropic for the electron its purity revives to $1/3$. On the other hand, the anisotropic HH revives to $\sim 2/3$.

For $r > 1$, as the external field increases, the Zeeman interaction becomes greater than the hyperfine interaction. The Zeeman induced coherent spin precession averages the influence of the hyperfine interaction perpendicular to the field, effectively reducing γ_y and γ_z . This effect can be viewed as a natural dynamical decoupling. This in turn results in temporal oscillations of the central spin purity. The frequency of these oscillations increases linearly with r while their amplitude decays. In addition, the spin revival peak reduces with the field as the effective ratio $\gamma_z / (\gamma_x + \gamma_y + \gamma_z)$ decreases. In the limit $r \gg 1$, the temporal dependence of the spin purity decay can be expressed analytically as $|S(t)| = e^{-\frac{1}{2}(\frac{\gamma_x}{\hbar}t)^2}$ depending only on the hyperfine interaction parallel to the field direction (see SM).

In summary, we present a comprehensive theoretical study of a central spin evolution interacting with nuclear spins in its vicinity, in the presence of externally applied magnetic field. Our studies are compared with comprehensive experimental studies of the evolution of the electron and heavy-hole spins confined in the same semiconductor quantum dot. We show that the central spin model well-describes the measured spins evolution. For large external field the central spin coherence decays like a Gaussian depending only on the hyperfine interaction parallel to the field's direction. In lower fields, in which the Zeeman interaction is comparable in magnitude to the hyperfine interaction with the nuclear spins, the spin purity oscillates in time during its dephasing. Under these conditions the Zeeman interaction is also smaller than the radiative linewidth. This is essential for entangled light sources. Our comprehensive study is therefore an important step towards bringing quantum dots based indistinguishable and entangled photon sources closer to real applications.

The support of the Israeli Science Foundation (ISF), and that of the European Research Council (ERC) under the European Union's Horizon 2020 research and innovation programme (Grant Agreement No. 695188) are gratefully acknowledged.

* dg@physics.technion.ac.il

- [1] J. P. Reithmaier, G. Şek, A. LSöffler, C. Hofmann, S. Kuhn, S. Reitzenstein, L. V. Keldysh, V. D. Kulakovskii, T. L. Reinecke, and A. Forchel, *Nature* **432**, 197 (2004).
- [2] T. Yoshie, A. Scherer, J. Hendrickson, G. Khitrova, H. M. Gibbs, G. Rupper, C. Ell, O. B. Shchekin, and D. G. Deppe, *Nature* **432**, 200 (2004).
- [3] M. Arcari, I. SSöllner, A. Javadi, S. L. Hansen, S. Mahmoodian, J. Liu, H. Thyrestrup, E. Lee, J. Song, S. Stobbe, and P. Lodahl, *Physical Review Letters* **113** (2014), 10.1103/physrevlett.113.093603.
- [4] P. Senellart, G. Solomon, and A. White, *Nature Nanotechnology* **12**, 1026 (2017).
- [5] D. Najer, I. SSöllner, P. Sekatski, V. Dolique, M. C. LSöbl, D. Riedel, R. Schott, S. Starosielec, S. R. Valentin, A. D. Wieck, N. Sangouard, A. Ludwig, and R. J. Warburton, *Nature* **575**, 622 (2019).
- [6] N. Somaschi, V. Giesz, L. D. Santis, J. C. Loredó, M. P. Almeida, G. Hornecker, S. L. Portalupi, T. Grange, C. Antón, J. Demory, C. Gómez, I. Sagnes, N. D. Lanzillotti-Kimura, A. Lemaitre, A. Auffeves, A. G. White, L. Lanco, and P. Senellart, *Nature Photonics* **10**, 340 (2016).
- [7] A. V. Kuhlmann, J. Houel, A. Ludwig, L. Greuter, D. Reuter, A. D. Wieck, M. Poggio, and R. J. Warburton, *Nature Physics* **9**, 570 (2013).
- [8] X. Ding, Y. He, Z.-C. Duan, N. Gregersen, M.-C. Chen, S. Unsleber, S. Maier, C. Schneider, M. Kamp, S. Höfling, C.-Y. Lu, and J.-W. Pan, *Physical Review Letters* **116** (2016), 10.1103/physrevlett.116.020401.
- [9] J. Kim, O. Benson, H. Kan, and Y. Yamamoto, *Nature* **397**, 500 (1999).
- [10] N. Akopian, N. H. Lindner, E. Poem, Y. Berlatzky, J. Avron, D. Gershoni, B. D. Gerardot, and P. M. Petroff, *Physical Review Letters* **96** (2006), 10.1103/physrevlett.96.130501.
- [11] R. Winik, D. Cogan, Y. Don, I. Schwartz, L. Gantz, E. R. Schmidgall, N. Livneh, R. Rapaport, E. Buks, and D. Gershoni, *Physical Review B* **95** (2017), 10.1103/physrevb.95.235435.
- [12] M. Zwerger, W. Dür, and H. J. Briegel, *Physical Review A* **85** (2012), 10.1103/physreva.85.062326.
- [13] W. J. Munro, A. M. Stephens, S. J. Devitt, K. A. Harrison, and K. Nemoto, *Nature Photonics* **6**, 777 (2012).
- [14] K. Azuma, K. Tamaki, and H.-K. Lo, *Nature Communications* **6** (2015), 10.1038/ncomms7787.
- [15] D. Buterakos, E. Barnes, and S. E. Economou, *Physical Review X* **7** (2017), 10.1103/physrevx.7.041023.
- [16] N. H. Lindner and T. Rudolph, *Physical Review Letters* **103**, (2009).
- [17] S. E. Economou, N. Lindner, and T. Rudolph, *Physical Review Letters* **105** (2010), 10.1103/physrevlett.105.093601.

- [18] I. Schwartz, D. Cogan, E. R. Schmidgall, Y. Don, L. Gantz, O. Kenneth, N. H. Lindner, and D. Gershoni, *Science* **354**, 434 (2016).
- [19] M. Bayer, G. Ortner, O. Stern, A. Kuther, A. A. Gorbunov, A. Forchel, P. Hawrylak, S. Fafard, K. Hinzler, T. L. Reinecke, S. N. Walck, J. P. Reithmaier, F. Klopff, and F. Schäfer, *Physical Review B* **65**, (2002).
- [20] D. Cogan, O. Kenneth, N. H. Lindner, G. Peniakov, C. Hopfmann, D. Dalacu, P. J. Poole, P. Hawrylak, and D. Gershoni, *Physical Review X* **8** (2018), 10.1103/physrevx.8.041050.
- [21] A. Kiraz, M. Atatüre, and A. Imamoglu, *Physical Review A* **69** (2004), 10.1103/physreva.69.032305.
- [22] L. Gantz, D. Cogan, I. Schwartz, E. Schmidgall, G. Bahir, and D. Gershoni, in *Conference on Lasers and Electro-Optics* (OSA, 2017).
- [23] A. Bechtold, D. Rauch, F. Li, T. Simmet, P.-L. Ardel, A. Regler, K. Muller, N. A. Sinitsyn, and J. J. Finley, *Nature Physics* **11**, 1005 (2015).
- [24] H. Bluhm, S. Foletti, I. Neder, M. Rudner, D. Mahalu, V. Umansky, and A. Yacoby, *Nature Physics* **7**, 109 (2010).
- [25] P.-F. Braun, X. Marie, L. Lombez, B. Urbaszek, T. Amand, P. Renucci, V. K. Kalevich, K. V. Kavokin, O. Krebs, P. Voisin, and Y. Masumoto, *Physical Review Letters* **94**, (2005).
- [26] B. D. Gerardot, D. Brunner, P. A. Dalgarno, P. Öhberg, S. Seidl, M. Kroner, K. Karrai, N. G. Stoltz, P. M. Petroff, and R. J. Warburton, *Nature* **451**, 441 (2008).
- [27] D. Brunner, B. D. Gerardot, P. A. Dalgarno, G. Wüst, K. Karrai, N. G. Stoltz, P. M. Petroff, and R. J. Warburton, *Science* **325**, 70 (2009).
- [28] B. Eble, C. Testelin, P. Desfonds, F. Bernardot, A. Balocchi, T. Amand, A. Miard, A. Lemaître, X. Marie, and M. Chamarro, *Physical Review Letters* **102**, (2009).
- [29] F. Fras, B. Eble, P. Desfonds, F. Bernardot, C. Testelin, M. Chamarro, A. Miard, and A. Lemaître, *Physical Review B* **84**, (2011).
- [30] K. De Greve, P. L. McMahon, D. Press, T. D. Ladd, D. Bisping, C. Schneider, M. Kamp, L. Worschech, S. Höfling, A. Forchel, and Y. Yamamoto, *Nature Physics* **7**, 872 (2011).
- [31] Y. Li, N. Sinitsyn, D. L. Smith, D. Reuter, A. D. Wieck, D. R. Yakovlev, M. Bayer, and S. A. Crooker, *Physical Review Letters* **108**, (2012).
- [32] J. H. Prechtel, A. V. Kuhlmann, J. Houel, A. Ludwig, S. R. Valentin, A. D. Wieck, and R. J. Warburton, *Nature Materials* **15**, 981 (2016).
- [33] D. Gammon, A. L. Efros, T. A. Kennedy, M. Rosen, D. S. Katzer, D. Park, S. W. Brown, V. L. Korenev, and I. A. Merkulov, *Physical Review Letters* **86**, 5176 (2001).
- [34] I. A. Merkulov, A. L. Efros, and M. Rosen, *Physical Review B* **65**, 205309 (2002).
- [35] A. V. Khaetskii, D. Loss, and L. Glazman, *Physical Review Letters* **88**, (2002).
- [36] J. Fischer, W. A. Coish, D. V. Bulaev, and D. Loss, *Physical Review B* **78**, 155329 (2008).
- [37] D. Cogan, G. Peniakov, Z.-E. Su, and D. Gershoni, *Physical Review B* **101** (2020), 10.1103/physrevb.101.035424.
- [38] W. D. Knight, *Physical Review* **76**, 1259 (1949).
- [39] A. W. Overhauser, *Physical Review* **92**, 411 (1953).
- [40] E. Barnes and S. E. Economou, *Physical Review Letters* **107**, (2011).
- [41] S. G. Carter, S. E. Economou, A. Greilich, E. Barnes, T. Sweeney, A. S. Bracker, and D. Gammon, *Physical Review B* **89**, (2014).

Supplemental material for “The coherence of quantum dot confined electron- and hole-spin in low external magnetic field”

Dan Cogan,¹ Zu-En Su,¹ Oded Kenneth,¹ and David Gershoni^{1, *}

¹The Physics Department and the Solid State Institute,
Technion–Israel Institute of Technology, 3200003 Haifa, Israel

We describe the temporal evolution of the polarization of a QD confined central electronic spin in the presence of an externally applied magnetic field and the influence of the nuclear spins, which comprise the QD and its vicinity. As the central-spin, we consider either an electron or a heavy hole.

As both cases involve a two-level spin system (a qubit), they may be described using the Pauli matrices $\sigma_x, \sigma_y, \sigma_z$, and the effective Hamiltonian must take the form

$$H = \frac{1}{2} \vec{C} \cdot \hat{\sigma}, \quad (1)$$

for some vector $\vec{C} = \vec{C}^{hf} + \vec{C}^{Zeeman}$ describing the spin’s hyperfine interaction with the QD nuclei and the Zeeman interaction with the external magnetic field. The exact expression of \vec{C} is different, of course, for each type of central spin.

The hyperfine interaction between the central spin and the effective magnetic (Overhauser) field generated by the $\sim 10^5$ nuclear spins in the QD is defined by

$$\vec{C}^{hf} = \bar{g} \mu_B \vec{B}_N,$$

where \bar{g} and μ_B are the central spin’s lande-factor tensor and Bohr magneton, and \vec{B}_N is the Overhauser field. The Overhauser field depends on the nature of the interaction between the spin and the nuclear environment [1–3].

Assuming that different nuclear spins are not correlated allows one to treat $\vec{B}_N(t)$ as having isotropic Gaussian random distribution satisfying

$$\langle \vec{B}_N \rangle = 0, \quad \langle B_{Nx}^2 \rangle = \langle B_{Ny}^2 \rangle = \langle B_{Nz}^2 \rangle = \sigma^2, \quad (2)$$

where σ is the width of the Gaussian distribution [1] (not to be confused with the Pauli matrices).

It is then convenient to define a modified unitless magnetic field $\vec{B} = \vec{B}_N / \sigma$ with root mean square of one and absorb σ into a redefined tensor $\bar{\gamma}$ having energy units. $H^{hf} = \frac{1}{2} \vec{C}^{hf} \cdot \hat{\sigma}$ then express the spin’s hyperfine interaction with $\vec{C}_e^{hf} = \bar{\gamma} \vec{B}$ where $\bar{\gamma} = \bar{g} \mu_B \sigma$ is the spin hyperfine coupling tensor.

While for the conduction electron, which has s-wave molecular symmetry the hyperfine tensor is approximately a scalar: [1]

$$\bar{\gamma}_e = \begin{pmatrix} \gamma_e & & \\ & \gamma_e & \\ & & \gamma_e \end{pmatrix},$$

for the heavy hole, this tensor is approximated by a diagonal but anisotropic tensor [2]

$$\bar{\gamma}_h = \begin{pmatrix} \gamma_{h_p} & & \\ & \gamma_{h_p} & \\ & & \gamma_{h_z} \end{pmatrix},$$

where the in-plane coupling component γ_{h_p} does not strictly vanish for the heavy-hole due its mixing with the light-hole [2]. Thus $\gamma_{h_z} > \gamma_{h_p}$.

Strictly speaking, the normalized Overhauser \vec{B} field that the hole feels maybe different than the field that the electron does. This is due to differences in the interaction of the electron and the hole spins with the nuclei. For our purpose, however, it is sufficient that the fields have the same Gaussian statistics. For the moment, we allow the functional relation between \vec{C} and \vec{B} to be arbitrary, and since our discussion is independent of these relations, it applies to both cases.

The Zeeman interaction between the central spin and an externally applied magnetic field \vec{B}_{ext} , is given by

$$\vec{C}^{zeeman} = \bar{g} \mu_B \vec{B}_{ext}. \quad (3)$$

It is fairly customary to assume that \bar{g} , the Lande-factor tensor describing the Zeeman interaction, is diagonal in our QD for both the electron and the hole, and taking the external magnetic field along the x-direction, the total interaction then assumes the form of a vector, given by

$$[C_x, C_y, C_z]^{(electron)} = [g_e \mu_B B_{ext} + \gamma_e B_x, \gamma_e B_y, \gamma_e B_z], \quad (4)$$

$$[C_x, C_y, C_z]^{(hole)} = [g_h \mu_B B_{ext} + \gamma_{h_p} B_x, \gamma_{h_p} B_y, \gamma_{h_z} B_z], \quad (5)$$

for the electron and hole, respectively. In the following we use $g_e, g_h, \gamma_e, \gamma_{h_p}$, and γ_{h_z} as fitting parameters, to best describe all the experimental observations.

\vec{B} and \vec{C} can be treated as time-independent at short times, and one readily finds the solution 2b

$$\vec{S}(t) = \frac{\vec{S}_0 \cdot \vec{C}}{C^2} \vec{C} + \left(\vec{S}_0 - \frac{\vec{S}_0 \cdot \vec{C}}{C^2} \vec{C} \right) \cos \left(\frac{C}{\hbar} t \right) - \frac{\vec{S}_0 \times \vec{C}}{C} \sin \left(\frac{C}{\hbar} t \right), \quad (6)$$

where $\vec{S}_0 = \vec{S}(0)$ is the central spin initial value. One may rewrite this relation in the form $\vec{S}(t) = \bar{G}(t)\vec{S}_0$ where $\bar{G}(t)$ is a 3×3 tensor whose elements can be easily read of Eq. 6.

The above relation may be interpreted either as a relation between (Heisenberg picture) operators or as a relation between their expectation values. In the following, it will be more convenient to take the latter point of view. (Note that the expectation value $\langle \vec{S} \rangle$ contains complete information about the quantum state for a two-state system.)

The probability distribution of B takes the standard form

$$dP = \frac{1}{(2\pi)^{3/2}} \exp\left(-\frac{1}{2}B^2\right) d^3B. \quad (7)$$

So the averaged spin is given by

$$\langle \vec{S}(t) \rangle = \left[\int \bar{G}(t) dP \right] \vec{S}_0 = \mathbf{G}(t) \vec{S}_0,$$

where $\mathbf{G}(t) = \int \bar{G}(t) dP$.

Under these assumptions, one may employ symmetries under reflections of the Overhauser field to show that the 3×3 tensor $\mathbf{G}(t)$ simplifies (basically due to the vanishing of odd integrals) into the form

$$\mathbf{G}(t) = \begin{bmatrix} \mathbf{G}_{xx}(t) & & \\ & \mathbf{G}_{yy}(t) & \mathbf{G}_{yz}(t) \\ & -\mathbf{G}_{yz}(t) & \mathbf{G}_{zz}(t) \end{bmatrix} \quad (8)$$

with

$$\begin{aligned} \mathbf{G}_{xx}(t) &= \int \frac{1}{C^2} \left[C_x^2 + (C_y^2 + C_z^2) \cos\left(\frac{C}{\hbar}t\right) \right] dP, \\ \mathbf{G}_{yy}(t) &= \int \frac{1}{C^2} \left[C_y^2 + (C_x^2 + C_z^2) \cos\left(\frac{C}{\hbar}t\right) \right] dP, \\ \mathbf{G}_{zz}(t) &= \int \frac{1}{C^2} \left[C_z^2 + (C_x^2 + C_y^2) \cos\left(\frac{C}{\hbar}t\right) \right] dP, \\ \mathbf{G}_{yz}(t) &= - \int \frac{C_x}{C} \sin\left(\frac{C}{\hbar}t\right) dP. \end{aligned} \quad (9)$$

We solve the integrals in Eq. 9 numerically with the parameters of Table. 1. We compare the results of the spin evolution measurements in Fig. 2 for the electron and Fig. 3 for the hole with our model for several Zeeman-hyperfine interaction ratio's r defined by

$$r = C_{zeeman}/C_{hf}^\perp = \frac{g_x \mu_B B_{ext}}{\sqrt{\gamma_y^2 + \gamma_z^2}}. \quad (10)$$

There is a good agreement between the model and the measured results.

The PL measurements in Figs. 2a-2b and Figs. 3a-3b are fitted with [4]

$$\begin{aligned} I_{+Z}(t) &= I(0) \exp(-t/\tau_{photon}) (1 - S_z(t)) \\ I_{-Z}(t) &= I(0) \exp(-t/\tau_{photon}) (1 + S_z(t)), \end{aligned}$$

where τ_{photon} is the radiative time of the Trion-HH optical transition, $I(0)$ is the initial emission intensity, and $I_{+Z}(t)$ ($I_{-Z}(t)$) denotes the measured PL intensity projected on right-hand (left-hand) circular polarization. $S_z(t)$ is the z component of the trion spin at time t, calculated numerically using Eq. 9 with the values of Table. 1 for the electron. There is a good agreement between the model and the measured results.

Next, we expand Eq. 9 in the limit of high external magnetic field $B_{ext} \gg \gamma/(g\mu_B)$ or $r \gg 1$. In this limit, The tensor $\mathbf{G}(t)$ is given by

$$\begin{aligned} \mathbf{G}_{xx}(t) &= 1 - \frac{1}{r^2} \left(1 - \cos(\omega_0 t) e^{-\frac{1}{2} \left(\frac{t}{T_2}\right)^2} \right) \\ &\quad + O(B_{ext}^{-3}) \\ \mathbf{G}_{yy}(t) &= e^{-\frac{1}{2} \left(\frac{t}{T_2}\right)^2} \cos(\omega_0 t) \\ &\quad - e^{-\frac{1}{2} \left(\frac{t}{T_2}\right)^2} \frac{\omega_0}{r^2} t \sin(\omega_0 t) + O(B_{ext}^{-2}) \\ \mathbf{G}_{zz}(t) &= e^{-\frac{1}{2} \left(\frac{t}{T_2}\right)^2} \cos(\omega_0 t) \\ &\quad - e^{-\frac{1}{2} \left(\frac{t}{T_2}\right)^2} \frac{\omega_0}{r^2} t \sin(\omega_0 t) + O(B_{ext}^{-2}) \\ \mathbf{G}_{yz}(t) &= -e^{-\frac{1}{2} \left(\frac{t}{T_2}\right)^2} \sin(\omega_0 t) \\ &\quad - e^{-\frac{1}{2} \left(\frac{t}{T_2}\right)^2} \frac{\omega_0}{r^2} t \cos(\omega_0 t) + O(B_{ext}^{-2}), \end{aligned} \quad (11)$$

where $\omega_0 = \frac{g\mu_B B_{ext}}{\hbar}$ is the Zeeman frequency, r is the Zeeman-hyperfine ratio parameter, defined in Eq. 10, and T_2 is the spin decay time.

In this large external field limit the total effective field \vec{C} is almost parallel to the x-axis, and therefore the corresponding spin component S_x remains almost unchanged (i.e. $G_{xx} \simeq 1$) while S_y, S_z decay at late times to a value $\sim \frac{C_y^2}{C^2} \sim \frac{\gamma_{yz}^2}{(g\mu_B B_{ext})^2} \ll 1$. The typical time scale for this decay is controlled by the random variations in the rotation frequency $\omega = \frac{C}{\hbar} = \frac{g\mu_B B_{ext}}{\hbar} + \frac{\gamma_x B_x}{\hbar} + O(\gamma^2)$. The central spin's purity $|S(t)| = \sqrt{S_x^2(t) + S_y^2(t) + S_z^2(t)}$ decay time in the limit of high external field is thus given by

$$T_2 = \frac{\hbar}{\gamma_x},$$

or in other words the purity decay time is inversely proportional to the hyperfine tensor component which is parallel to the externally applied magnetic field.

* dg@physics.technion.ac.il

- [1] I. A. Merkulov, A. L. Efros, and M. Rosen, *Physical Review B* **65**, 205309 (2002).
- [2] B. Eble, C. Testelin, P. Desfonds, F. Bernardot, A. Balocchi, T. Amand, A. Miard, A. Lemaitre, X. Marie, and M. Chamarro, *Physical Review Letters* **102**, (2009).
- [3] D. Cogan, O. Kenneth, N. H. Lindner, G. Peniakov, C. Hopfmann, D. Dalacu, P. J. Poole, P. Hawrylak, and D. Gershoni, *Physical Review X* **8** (2018), 10.1103/physrevx.8.041050.
- [4] D. Cogan, G. Peniakov, Z.-E. Su, and D. Gershoni, *Physical Review B* **101** (2020), 10.1103/physrevb.101.035424.